Langmuir

Article

pubs.acs.org/Langmuir

Effects of the Electrode Size and Modification Protocol on a Label-Free Electrochemical Biosensor

Sunil K. Arya,*[,†] Tze Sian Pui,[†] Chee Chung Wong,[†] Sai Kumar,[‡] and Abdur Rub Abdur Rahman[†]

[†]Bioelectronics Programme, Institute of Microelectronics, A*STAR (Agency for Science, Technology and Research), 11 Science Park Road, Singapore Science Park II, Singapore 117685

[‡]SFC Fluidics LLC, Enterprise Center, 534 West Research Center Boulevard, Suite 260, Arkansas Research and Technology Park, Fayetteville, Arkansas 72701, United States

Supporting Information

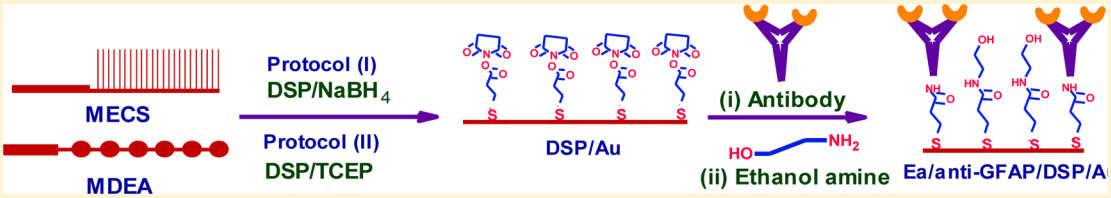

ABSTRACT: In the present work, the effect of a surface modification protocol along with the electrode size has been investigated for developing an efficient, label-free electrochemical biosensing method for diagnosis of traumatic brain injury (TBI) biomarkers. A microdisk electrode array (MDEA) and a macroelectrode with a comb structure (MECS) were modified with an anti-GFAP (GFAP = glial fibrillary acidic protein) antibody using two protocols for optimum and label-free detection of GFAP, a promising acute-phase TBI biomarker. For the MDEA, an array of six microdisks with a 100 μm diameter and, for the MECS, a 3.2 mm × 5.5 mm electrode 5 μm wide with 10 μm spaced comb fingers were modified using an optimized protocol for dithiobis(succinimidyl propionate) (DSP) self-assembled monolayer formation. Anti-GFAP was covalently bound, and the remaining free DSP groups were blocked using ethanolamine (Ea). Sensors were exposed to solutions with different GFAP concentrations, and a label-free electrochemical impedance spectroscopy (EIS) technique was used to determine the concentration. EIS results confirmed that both types of Ea/anti-GFAP/DSP/Au electrodes modified with an optimized DSP-based protocol can accurately detect GFAP in the range of 1 pg mL^{-1} to 100 ng mL^{-1} with a detection limit of 1 pg mL^{-1}. However, the cross-use of the MDEA protocol on the MECS and vice versa resulted in very low sensitivity or poor signal resolution, underscoring the importance of proper matching of the electrode size and type and the surface modification protocol.

INTRODUCTION

Traumatic brain injury (TBI) is a predominant cause of death and morbidity in children and adolescents.[1−7] TBI not only involves the initial injury event of varying severity, but is often followed by a destructive cascade of secondary cell death within the injured core that spreads into adjacent brain tissue over time.[5,8] Therefore, there is a need for development of a suitable technique for TBI detection. Currently, TBI diagnoses are made by tests such as magnetic resonance imaging (MRI), computed tomography (CT) scans, diffusion tensor imaging (DTI), or in-hospital observation.[3,5−7] However, these are expensive, impractical in resource-constrained environments, involve potentially harmful ionizing radiation, and require advanced expertise.[4,6,9] Studies have indicated that the cell death occurring after TBI results in the release of various brain proteins into biofluids.[10−14] The pattern and timing of post-TBI release for such protein biomarkers in biofluids can provide information of injury magnitude and outcome. Among various markers for TBI, glial fibrillary acidic protein (GFAP) is specific to brain tissue and released only after astrocyte death.[15−17] Papa et al. have shown increased levels of GFAP protein in serum samples from human mild to moderate TBI patients. In their enzyme-linked immunosorbent assay (ELISA)-based study, they were able to detect GFAP in serum within 1 h of injury, with a lower limit of detection at 0.02 ng mL^{-1}.[3] In another study by Vos et al., using a distinct ELISA protocol, GFAP levels in serum predicted mortality and unfavorable outcome at a cutoff of 1.5 ng mL^{-1}.[18] Moreover, current evidence indicates that serum GFAP is a useful marker for various types of brain damage and its serum levels correlate with injury severity and outcome.[1,3−5,17−20] Therefore, there is enormous diagnostic and prognostic promise in developing assays that measure the GFAP biomarker levels in an accurate and timely manner.

Recently, electrochemical biosensors, capable of a direct transduction of the biomolecular recognition event into an electronic signal, enabling lower detection limits are gaining interest for sensitive and specific detection of a target analyte.[21−23] However, to realize a biosensor with improved parameters such as selectivity and stability, which depend on

Received: March 24, 2013
Revised: May 2, 2013

   dx.doi.org/10.1021/la401109r | Langmuir XXXX, XXX, XXX−XXX

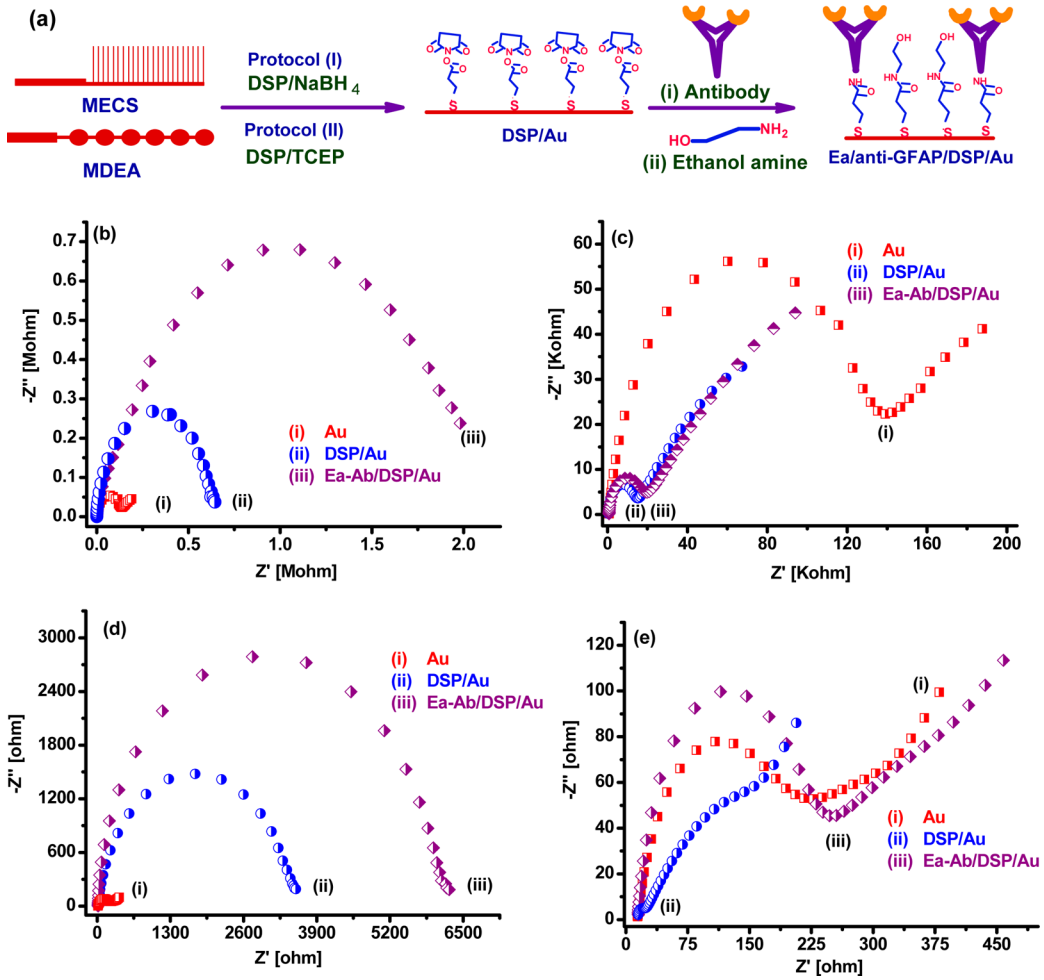

Figure 1. (a) Schematic for Ea/anti-GFAP/DSP/MDEA and Ea/anti-GFAP/DSP/MECS bioelectrode fabrication. (b–e) EIS spectra for the (b) MDEA and P-I, (c) MDEA and P-II, (d) MECS and P-I, and (e) MECS and P-II.

the biosensing molecule attachment and its compatibility with the solid surface, requires extensive investigations.[24−27] Biosensor development using self-assembled monolayers (SAMs) and electrochemical techniques has recently been employed, where SAM formation allows the binding of biomolecules in the closest vicinity of the electrode surface, and the electrochemical detection technique results in enhanced sensitivity, fast response, low cost, and portability.[22,28,29] Moreover, SAMs are easy to form, and the properties of SAMs can be easily manipulated via changing the functional groups to those compatible for the immobilization of biomolecules. However, binding of biomolecule on a SAM usually requires either activation or further modification that might disturb the integrity of the SAM or biomolecule, resulting in its denaturation and loss of activity.[30,31] In this context, dithiobis(succinimidyl propionate) (DSP), which can act as a binder of biomolecules onto the gold surface via SAM formation through chemisorption and biomolecule binding via the terminal succinimidyl group present on the surface of the DSP SAM, has recently received interest as an immobilization matrix.[23,32,33]

Presently, large macroelectrodes are commonly used with SAMs to fabricate biosensors.[30,32] However, studies have indicated that use of a microelectrode can offer several benefits over that of larger area macroelectrodes, such as higher sensitivity with minimum variability due to a radial diffusion profile as opposed to a planar diffusion profile in macroelectrodes.[28,34,35] To the best of our knowledge, there are no reports on the comparison of data obtained from use of macro- and microelectrodes with a DSP-SAM-based biomolecule immobilization protocol for optimum response. In this work, two different electrodes in the form of a microdisk electrode array (MDEA) and a macroelectrode with a comb structure (MECS) have been investigated with two different DSP modification protocols for optimum, ultrasensitive, and label-free electrochemical assay of GFAP. This work demonstrates that proper matching of the selected electrode size with the protocol results in high sensitivity and signal resolution, whereas inappropriate (cross) matching of the electrode size with the protocol results in very low sensitivity or poor signal resolution. The optimized biosensor, using an electrochemical impedance technique, proved the feasibility of GFAP detection in the clinically relevant range of 1 pg mL^{-1} to 100 ng mL^{-1}, with a detection limit of 1 pg mL^{-1}.

2. MATERIALS AND METHODS

2.1. Chemicals and Reagents. DSP was procured from Proteochem. Anti-GFAP antibody and GFAP antigen were purchased from Abnova. Phosphate buffer solution (PBS; pH 7.4) was obtained from Invitrogen, Grand Island, NY. Dimethylsulfoxide (DMSO) and tris(2-carboxyethyl)phosphine hydrochloride (TCEP) solution were procured from Sigma. All other chemicals were of analytical grade and

dx.doi.org/10.1021/la401109r | Langmuir XXXX, XXX, XXX−XXX

used without purification. Working solutions of GFAP were prepared by dilution in PBS.

2.2. Measurement and Apparatus. Electrochemical impedance spectroscopy (EIS) was utilized to characterize the Ea/anti-GFAP/DSP/Au (Ea = ethanolamine) bioelectrode and to estimate the GFAP concentration. EIS is a powerful and sensitive tool for studying the charge transfer processes occurring at electrode−solution or modified electrode−solution interfaces. In the Nyquist plot of the impedance spectra, the usually observed semicircle corresponds to the electron-transfer resistance process (R_{ct}). The magnitude of R_{ct} depends on the dielectric and insulating features at the electrode−electrolyte interface and can be used to interpret electrode−electrolyte interface properties.

EIS measurements were carried out in the frequency range of 0.5 Hz to 500 kHz with a 25 mV amplitude using an Autolab potentiostat/galvanostat (Eco Chemie, The Netherlands). EIS measurements were carried out using 15 and 60 μL PBS solutions (10 mM, pH 7.4) containing a mixture of 5 mM $Fe(CN)_6^{4-}$ (ferrocyanide) and 5 mM $Fe(CN)_6^{3-}$ (ferricyanide), i.e., 5 mM $Fe(CN)_6^{3-/4-}$, as a redox probe on the MDEA and MECS, respectively, in a three-electrode configuration with gold as the counter and pseudo reference electrodes. Experiments were carried out in triplicate, and an Autolab frequency response analyzer, version 4.9.006, was used to assess charge transfer resistance values.

Contact angle measurements were conducted to check the hydrophilic/hydrophobic nature of the surface before and after modification and the immobilization of antibody by the sessile drop method using a drop shape analyzer (DSA 100) from Kruss Gmbh, Hamburg, Germany.

2.2. Gold Electrode and Ea/Anti-GFAP/DSP/Au Bioelectrode Fabrication. The MDEA and MECS were fabricated on an oxidized silicon wafer using standard microfabrication techniques as described in an earlier paper.[28] For the MDEA, an array of six microdisks with a 100 μm diameter and, for the MECS, a 3.2 mm × 5.5 mm electrode 5 μm wide with 10 μm spaced comb fingers were fabricated and utilized.

The fabricated electrodes were precleaned with acetone, ethanol, and copious amounts of deionized water. The electrodes were cleaned again with oxygen plasma for 10 min before use. The electrodes were modified with DSP using two different protocols (Figure 1). Protocol I (P-I): A 2 mg mL^{-1} DSP solution in acetone was first reduced for 10 min at room temperature using 10 mg mL^{-1} $NaBH_4$ solution in deionized water. For reduction 5 μL of $NaBH_4$ solution was added per milliliter of DSP solution. The electrodes were then incubated in reduced DSP solution for SAM formation for 2 h on a shaker at 50 rpm. Protocol II (P−II): A 2 mg mL^{-1} DSP solution in DMSO was first reduced for 10 min at room temperature using 0.5 M TCEP solution. For reduction 10 μL of TCEP solution was added per milliliter of DSP solution. The electrodes were then incubated in reduced DSP solution for SAM formation for 1 h on a shaker at 50 rpm. Two different reducing agents ($NaBH_4$ and TCEP) in two different media resulted in reduction and breaking of the disulfide bond to different extents, thus producing SAMs with different properties (Figure 1). Before using these optimized amounts, the volume and time for DSP and reducing agents, a large number of iterations were tested, and the present work describes only the optimum values under which the best results and comparison were observed. The DSP-SAM-modified electrodes were then rinsed with acetone/DMSO to remove any unbound DSP followed by water rinsing and drying under nitrogen gas.

GFAP antibodies were covalently attached to the DSP SAM by incubating the electrode in 15 and 50 μL of 2 μg mL^{-1} antibody in PBS solution (10 mM, pH 7.4) for 1 h on the MDEA and MECS, respectively. Covalent binding (amide bond formation) results from the facile reaction between the amino group of the antibody and the reactive succinimidyl group of DSP on the SAM surface (Figure 1). The bioelectrode was washed thoroughly with PBS to remove any unbound biomolecules followed by a 10 min washing with 10% ethanolamine solution in PBS. Ethanolamine was used to block unreacted succinimidyl groups on the DSP SAM and to remove extra unbound antibodies on the electrode surface.

3. RESULTS AND DISCUSSION

3.1. Ea/Anti-GFAP/DSP/MDEA and Ea/Anti-GFAP/DSP/MECS Bioelectrode Fabrication. Figure 1 shows the schematic of Ea/anti-GFAP/DSP/MDEA and Ea/anti-GFAP/DSP/MECS bioelectrode fabrication and EIS-based characterization. Nyquist plots of the impedance spectra were recorded after each step of the modification processes, and the diameter of the semicircle, i.e., R_{ct}, was estimated. From parts b−e of Figure 1, it is clear that the electrodes behave differently toward different protocols, indicating size and modification protocol dependence. In Figure 1b,d, an increase in R_{ct} for DSP SAM formation was observed, which reveals dielectric shielding of the electrode array by high-density DSP SAM formation using P-I. In contrast, for Figure 1c,e, which uses P-II, a decrease in R_{ct} upon DSP SAM formation was observed. The initial impedance of the blank MDEA was found to be very high and was attributed to the very small size of the electrode. A decrease in R_{ct} after SAM formation for P-II was found to be very surprising. The experiments were repeated on more than 10 chips, and the results were found to be consistent.

To understand the different behaviors with TCEP in P-II, various new EIS studies, including time variation (Supplementary Figure 1, Supporting Information) and the effect of different media [(i) buffer, (ii) DSP (P-II), 1 h (iii) DSP in DMSO, 1 h, (iv) DMSO with TCEP, 1 h, (v) DSP (P-I), 30 s (Supplementary Figure 2a, Supporting Information) and (i) DSP−$NaBH_4$−DMSO, 1 h, (ii) DSP (P-I), 3 min, (iii) DSP−TCEP−acetone, 1 h, and (iv) DSP (P-I), 2 h (Supplementary Figure 2b)], were performed (Supplementary data 1, Supporting Information). The results indicate that the time of incubation does not produce much affect, and the results of the different media study, where a decrease of R_{ct} was observed only in the P-II condition, suggest that DSP with TCEP in DMSO might form some sort of complex which may result in such behavior. Further investigation should be done in the future to understand the exact reason for this phenomenon; however, the change in R_{ct} indicates successful modification of the electrode surface. Cyclic voltammetric studies (Supplementary data 1, Supporting Information) also indicated the difference in DSP SAM formation for P-I and P-II. Furthermore, the increase in R_{ct} with P-I and decrease in R_{ct} with P-II clearly suggest the protocol dependence of SAM-based surface modification in both micro and macroelectrode structures.

Covalent binding of anti-GFAP followed by removal of physically adhered antibody and blocking of exposed succinimidyl groups on the DSP SAM via ethanolamine results in an increase of R_{ct} in each case. The increase in R_{ct} suggests successful fabrication of Ea/anti-GFAP/DSP/MDEA and Ea/anti-GFAP/DSP/MECS bioelectrodes and can be attributed to the binding of nonconducting antibody, which retards the charge transfer process, resulting in an increase of R_{ct}.

3.2. Contact Angle Studies for Ea/Anti-GFAP/DSP/Au Bioelectrode Fabrication Using P-I and P-II. To investigate Ea/anti-GFAP/DSP/Au bioelectrode fabrication using P-I and P-II, the contact angle measurements were carried out using the sessile drop method. The change in the value of the contact angle reveals the hydrophobic/hydrophilic character of the surface, which in turn can be related to DSP SAM layer formation and anti-GFAP immobilization on the gold surface. Figure 2 shows the contact angle images for freshly oxygen

dx.doi.org/10.1021/la401109r | Langmuir XXXX, XXX, XXX−XXX

Table 1. Quantitative R_{ct} Data for the MDEA with P-I, MDEA with P-II, MECS with P-I, and MECS with P-II

electrode	solution resistance (R_s, Ω)	charge transfer resistance (R_{ct})	n
	MDEA with P-I		
MDEA	700	131.3 kΩ	0.888
DSP/MDEA	690	1.23 MΩ	0.941
Ea/anti-GFAP/DSP/MDEA	650	1.83 MΩ	0.823
	MDEA with P-II		
MDEA	740	134.73 kΩ	0.89
DSP/MDEA	680	17.86 kΩ	0.959
Ea/anti-GFAP/DSP/MDEA	672	18.83 kΩ	0.907
	MECS with P-I		
MECS	14.7	212.2 Ω	0.873
DSP/MECS	15.3	3429.3 Ω	0.908
Ea/anti-GFAP/DSP/MECS	15	5866.4 Ω	0.969
	MECS with P-II		
MECS	14.6	200.1 Ω	0.845
DSP/MECS	14.2	13.3 Ω	0.866
Ea/anti-GFAP/DSP/MECS	15.6	215.4 Ω	0.954

plasma cleaned bare Au, DSP/Au, and EA/anti-GFAP/DSP/Au electrodes for P-I and P-II.

It can be seen that the value of the contact angle increases dramatically from 6° for bare Au to 34° and 25° for DSP/Au using P-I and P-II, respectively, indicating that the DSP molecules get adsorbed on the Au surface. Furthermore, the higher value in P-I suggests a larger surface coverage by DSP molecules. The decrease in the value of the contact angle to 18° and 17°, respectively, for P-I and P-II was observed after reaction with anti-GFAP. The observed decrease in the value of the contact angle suggests a hydrophilic nature of the surface, confirming the immobilization of anti-GFAP onto the DSP/Au surface. Measurements were repeated in triplicate on different chips, and the results were found within ±4°. Also atomic force microscopy (AFM) studies were carried out to investigate Ea/anti-GFAP/DSP/Au bioelectrode fabrication using P-I and P-II (Supplementary data 3, Supporting Information). The results suggest successful modification in both protocols.

3.3. GFAP Response Studies of the MDEA-Based Ea/Anti-GFAP/DSP/MDEA Bioelectrode. Figure 3 shows the EIS spectra obtained for GFAP concentrations in the 1 pg mL^{-1} to 100 ng mL^{-1} range on the MDEA-based Ea/anti-GFAP/DSP/MDEA bioelectrode using both protocols. For each concentration, the bioelectrode was incubated with 15 μL of GFAP solution for 30 min, followed by PBS washing and EIS spectrum recording. With increasing GFAP concentration, R_{ct} was found to increase regularly, indicating that GFAP binds to immobilized anti-GFAP on the bioelectrode, producing a packed layer that effectively decreases the electron transfer rate for the redox probe. However, from Figure 3a,c it is clear that the bioelectrode shows significantly better and uniform resolution of the signal at different concentrations when used with P-II, whereas for P-I, though an increase in the signal was observed, the resolution was very poor and intermediate concentrations could not be estimated because of signal overlap, thus suggesting a protocol-dependent response for MDEA.

For both protocols, a linear relationship between the R_{ct} values and the logarithm of the GFAP concentrations (1 pg mL^{-1} to 100 ng mL^{-1}) was observed, with the following regression equations: R_{ct} (Ω) = $(3.16 \times 10^6) + (9.3 \times 10^4)$ $\log[c_{GFAP}$ (g mL^{-1})] for P-I and R_{ct} (Ω) = $(3.15 \times 10^5) + (2.2 \times 10^4)$ $\log[c_{GFAP}$ (g mL^{-1})] for P-II. However, with P-I, a large deviation is visible in Figure 3b, indicating that P-II is more suitable for the MDEA. Furthermore, these MDEA-based bioelectrodes exhibited standard deviations of 1.64 and 0.68 with corresponding correlation coefficients of 0.982 and 0.997 for P-I and P-II, respectively. Imprecision of the data indicated by error bars in Figure 3b,d was found to be <5%.

3.4. GFAP Response Studies of the MECS-Based Ea/Anti-GFAP/DSP/MECS Bioelectrode. Figure 4 shows the EIS spectra obtained for GFAP concentrations of 1 pg mL^{-1} to 100 ng mL^{-1} on the MECS-based Ea/anti-GFAP/DSP/MECS bioelectrode using both protocols. For each concentration, the bioelectrode was incubated with 60 μL of GFAP solution for 30 min, followed by PBS washing and EIS spectrum recording. With increasing GFAP concentration, R_{ct} was found to increase regularly, indicating that GFAP binds to the immobilized anti-

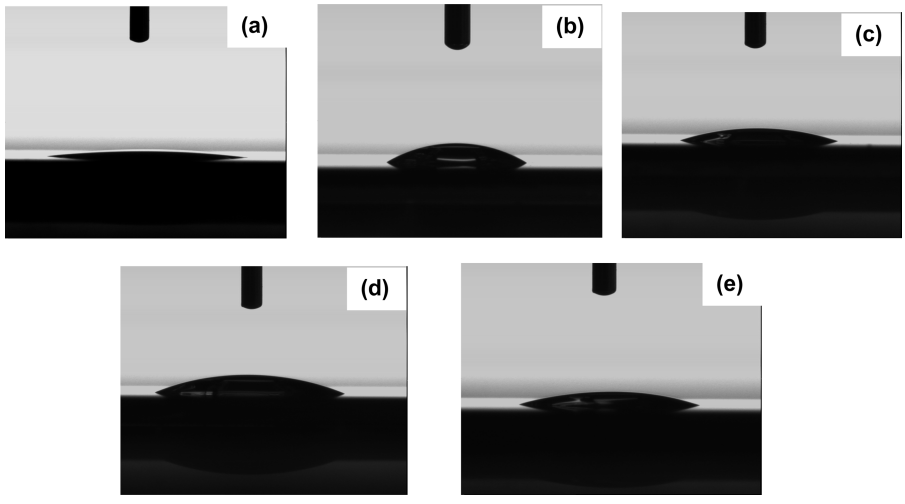

Figure 2. Contact angle images for (a) bare Au, (b) DSP/Au (P-I), (c) EA/anti-GFAP/DSP/Au (P-I), (d) DSP/Au (P-II), and (e) EA/anti-GFAP/DSP/Au (P-II) electrodes.

dx.doi.org/10.1021/la401109r | Langmuir XXXX, XXX, XXX−XXX

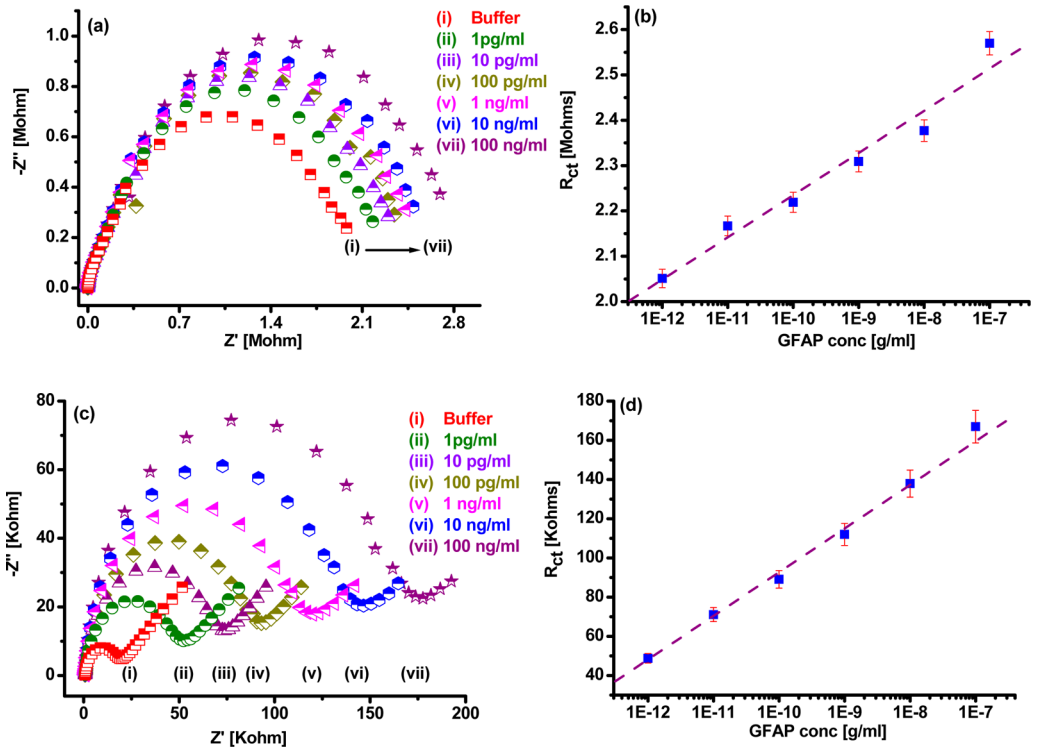

Figure 3. EIS spectra of the Ea/anti-GFAP/DSP/MDEA bioelectrode for different GFAP concentrations [(i) buffer, (ii) 1 pg mL^{-1}, (iii) 10 pg mL^{-1}, (iv) 100 pg mL^{-1}, (v) 1 ng mL^{-1}, (vi) 10 ng mL^{-1}, and (vii) 100 ng mL^{-1}] for the (a) MDEA and P-I and (c) MDEA and P-II. Curves b and d are linearity curves for data obtained from EIS studies (shown in (a) and (c), respectively) for different GFAP concentrations. The error bars indicate the results of triplicate experiments.

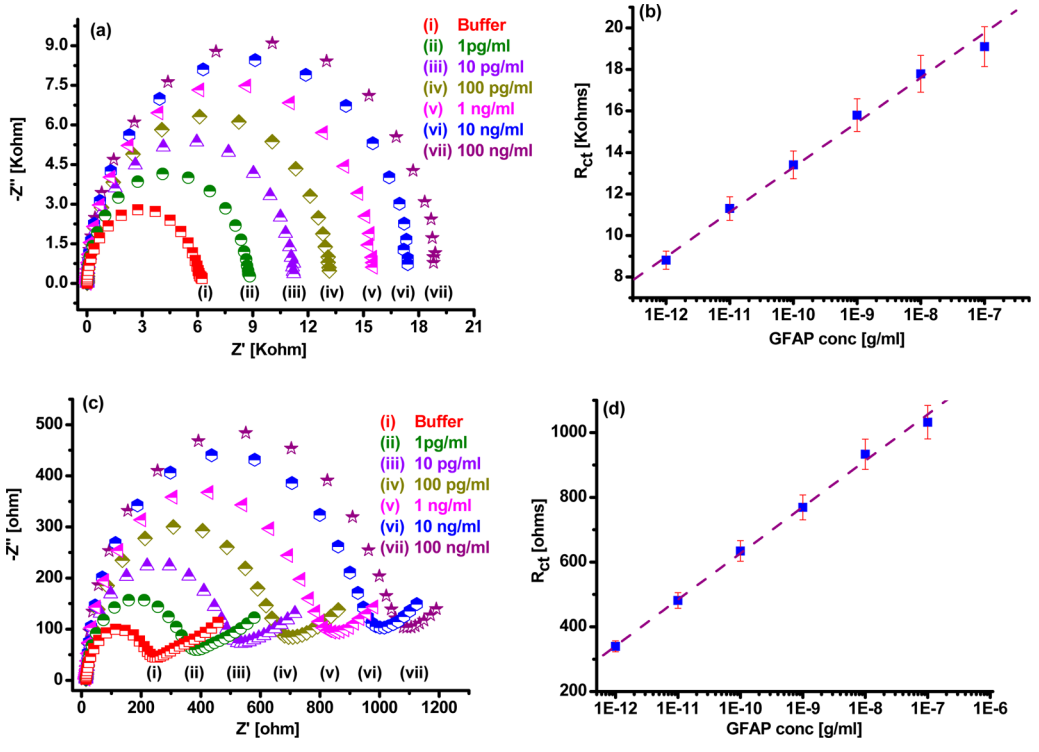

Figure 4. EIS spectra of the Ea/anti-GFAP/DSP/MECS bioelectrode for different GFAP concentrations [(i) buffer, (ii) 1 pg mL^{-1}, (iii) 10 pg mL^{-1}, (iv) 100 pg mL^{-1}, (v) 1 ng mL^{-1}, (vi) 10 ng mL^{-1}, and (vii) 100 ng mL^{-1}] for the (a) MECS and P-I and (c) MECS and P-II. Curves b and d are linearity curves for data obtained from EIS studies (shown in (a) and (c), respectively) for different GFAP concentrations. The error bars indicate the results of triplicate experiments.

dx.doi.org/10.1021/la401109r | *Langmuir* XXXX, XXX, XXX−XXX

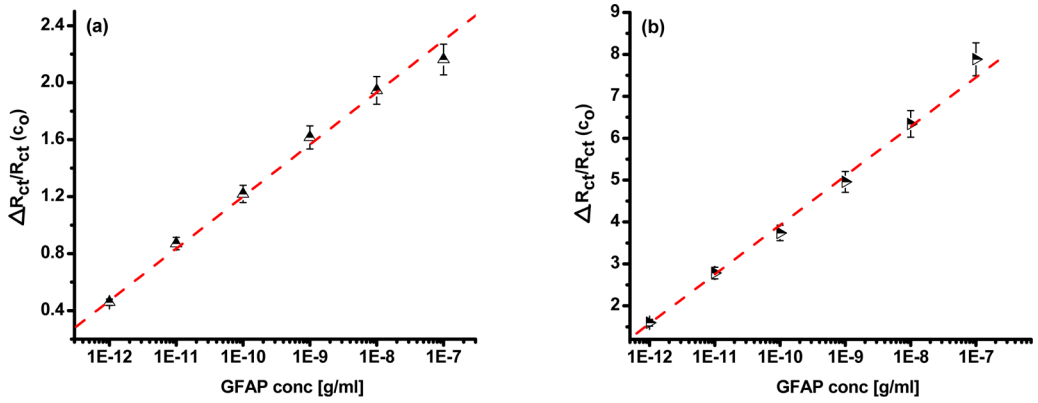

Figure 5. Curve between $\Delta R_{ct}/R_{ct}(c_o)$ and the concentration of GFAP for measurement of K_a of the (a) MECS with P-I and (b) MDEA with P-II.

GFAP on the bioelectrode, producing a packed layer that effectively reduces the electron transfer rate for the redox probe. From Figure 4a,c, it is clear that the bioelectrode shows resolvable signals at different concentrations of the analyte with both protocols. However, the value of R_{ct} for P-II (cf. Figure 4c) is very low, indicating ineffective surface modification of the bioelectrode. In contrast, for P-I, the relative change in R_{ct} is in kΩ, which translates to a very high sensitivity.

For both protocols, a linear relationship between the R_{ct} values and the logarithm of the GFAP concentrations (1 pg mL^{-1} to 100 ng mL^{-1}) was obtained and can be represented as regression equations: R_{ct} (Ω) = (3.5×10^4) + (2.2×10^3) log[c_{GFAP} (g mL^{-1})] for P-I and R_{ct} (Ω) = (2.1×10^3) + (1.4×10^2) log[c_{GFAP} (g mL^{-1})] for P-II. The MECS bioelectrode exhibited a sensitivity of 2.2×10^3 Ω (g mL^{-1})$^{-1}$ GFAP with P-I, which is 15 times higher than that obtained for P-II (1.4×10^2 Ω (g mL^{-1})$^{-1}$ GFAP). Furthermore, these bioelectrodes exhibited standard deviations of 0.495 and 0.342 with corresponding correlation coefficients of 0.997 and 0.999 for P-I and P-II, respectively. The imprecision of the data as indicated by the error bars in Figure 4b,d was found to be within 5%.

The results from Figures 3 and 4 clearly suggest that P-I is more suitable for the MECS, indicating that the SAM coverage obtained under the mentioned conditions is sufficient for effective Ea/anti-GFAP/DSP/MECS bioelectrode fabrication, which is further manifested by the fact that the R_{ct} of the DSP-modified MECS was very low when P-II was used, indicating low surface coverage by SAM formation. Furthermore, it resulted in very low sensitivity during measurement. Also the MECS was tested for P-I with ∼5 h and overnight SAM formation (data not shown), and it was found that ∼5 h or overnight SAM formation resulted in a very high density SAM, making the surface insulating. Furthermore, the Ea/anti-GFAP/DSP/MECS bioelectrode prepared using such a long time or overnight SAM resulted in a very insignificant response. Thus, low coverage of DSP via P-II and highly dense coverage by ∼5 h or overnight SAM formation resulted in a very poor signal, and an optimum response was observed only when P-I was used with 2 h of SAM formation. Similarly, P-II was found to be more suitable for the MDEA, indicating that SAM coverage obtained under the mentioned conditions is sufficient for effective Ea/anti-GFAP/DSP/MDEA bioelectrode fabrication. It is further manifested by the fact that R_{ct} of the DSP-modified MDEA was very high when P-I was used, which resulted in a very insulating Ea/anti-GFAP/DSP/MDEA bioelectrode exhibiting a very low signal resolution during measurement.

Thus, the optimum response is clearly dependent on the electrode size and modification protocol, and in the present work, P-I is more suitable for the MECS whereas P-II is more suitable for the MDEA to obtain the best performance of the bioelectrode.

3.5. Estimation of the Association Constant between the Covalently Bound Anti-GFAP and GFAP. The association constant (K_a) for binding interaction was determined using the Langmuir isotherm approach in which the isotherm assumes equal binding energy for all binding sites.[36,37] For K_a estimation, the change in R_{ct} was related to the binding of GFAP with immobilized anti-GFAP and is represented by the following equation:

$$M = 1 - \frac{R_{ct}(c_o)}{R_{ct}(c_i)} \tag{1}$$

where M, $R_{ct}(c_o)$, and $R_{ct}(c_i)$ indicate the number of occupied binding sites, charge transfer resistance without GFAP, and charge transfer resistance with the desired concentration of GFAP, respectively. In the Langmuir isotherm, M can be related to association constant using the following equation:

$$M = \frac{K_a c}{1 + K_a c} \tag{2}$$

where K_a is the association constant and c is the concentration of molecules in the solution. On rearrangement of eq 2, we get

$$K_a c = \frac{M}{1 - M} \tag{3}$$

From eqs 1 and 3

$$K_a c = \frac{R_{ct}(c_i) - R_{ct}(c_o)}{R_{ct}(c_o)} = \frac{\Delta R_{ct}}{R_{ct}(c_o)} \tag{4}$$

Using eq 4, the curve was plotted between $\Delta R_{ct}/R_{ct}(c_o)$ and the concentration of GFAP (Figure 5). Figure 5 reveals that $\Delta R_{ct}(c_i)/(R_{ct}(c_o)$ varies linearly with the concentration and follows the linear equation $\Delta R_{ct}(c_i)/R_{ct}(c_o) = 4.854 + 0.365 \log c_{GFAP}$ with a correlation coefficient of 0.998 and a standard deviation of 0.858 for the MECS with P-I and $\Delta R_{ct}(c_i)/(R_{ct}(c_o)] = 15.678 + 1.175 \log c_{GFAP}$ with a correlation coefficient of 0.998 and a standard deviation of 0.819 for the MDEA with P-II. K_a was estimated from the slope of the regression equation and found to be 0.365 mL/g for the MECS with P-I and 1.175 mL/g for the MDEA with P-II. The

dx.doi.org/10.1021/la401109r | Langmuir XXXX, XXX, XXX−XXX

observed different values further indicate the effect of the electrode and modification protocol.

4. CONCLUSIONS

In summary, the present work emphasizes the importance of the proper choice of surface modification protocol on sensors with different electrode geometries. To achieve the optimum response with high sensitivity and resolution, P-I involving DSP in acetone with $NaBH_4$ reduction was found to be more suitable for the MECS and P-II involving DSP in DMSO with TCEP reduction was found more suitable for the MDEA. Characterization of bioelectrode fabrication and GFAP concentration studies indicate that the electrode geometry needs proper matching with the surface modification protocol. Label-free GFAP detection using EIS techniques reveals that the Ea/anti-GFAP/DSP/Au-based biosensor fabricated with an appropriately matched and optimized protocol can accurately detect GFAP in the range of 1 pg mL^{-1} to 100 ng mL^{-1}. Furthermore, the MECS biosensor with the optimum protocol exhibited 15 times higher sensitivity, whereas the MDEA biosensor exhibited a higher signal resolution for each concentration. Thus, the electrode geometry, as well as the choice of surface modification protocol, is crucial for biosensor performance. This work mainly concentrates on demonstrating the effect of the electrode size and protocol of modification on bioelectrode fabrication. The detailed work required for biosensor fabrication for clinical application in TBI diagnostics, involving studies on the effect of interferents, the stability of the bioelectrode, and batch-to-batch variation of chip fabrication and selective detection and estimation of the sample in serum solution are in progress and will be published in the future.

■ ASSOCIATED CONTENT

Ⓢ Supporting Information

Description of various EIS studies performed to investigate the strange behavior of P-II based DSP SAM formation, cyclic voltammetric studies showing different SAM behaviors in P-I and P-II, and AFM studies revealing successful surface modification via P-I and P-II. This material is available free of charge via the Internet at http://pubs.acs.org/

■ AUTHOR INFORMATION

Corresponding Author

*Phone: +65 90702464. Fax: +65 64640517. E-mail: sunilarya333@gmail.com.

Notes

The authors declare no competing financial interest.

■ ACKNOWLEDGMENTS

This work was supported by the A*STAR (Agency for Science, Technology and Research), Singapore, Grant IME/12-330041.

■ REFERENCES

(1) Nylen, K.; Ost, M.; Csajbok, L. Z.; Nilsson, I.; Blennow, K.; Nellgard, B.; Rosengren, L. Increased serum-GFAP in patients with severe traumatic brain injury is related to outcome. *J. Neurol. Sci.* **2006**, *240* (1), 85−91.

(2) Zurek, J.; Fedora, M. The usefulness of S100B, NSE, GFAP, NF-H, secretagogin and Hsp70 as a predictive biomarker of outcome in children with traumatic brain injury. *Acta Neurochir.* **2012**, *154* (1), 93−103.

(3) Papa, L.; Lewis, L. M.; Falk, J. L.; Zhang, Z.; Silvestri, S.; Giordano, P.; Brophy, G. M.; Demery, J. A.; Dixit, N. K.; Ferguson, I.; Liu, M. C.; Mo, J.; Akinyi, L.; Schmid, K.; Mondello, S.; Robertson, C. S.; Tortella, F. C.; Hayes, R. L.; Wang, K. K. W. Elevated levels of serum glial fibrillary acidic protein breakdown products in mild and moderate traumatic brain injury are associated with intracranial lesions and neurosurgical intervention. *Ann. Emerg. Med.* **2012**, *59* (6), 471−483.

(4) Fraser, D. D.; Close, T. E.; Rose, K. L.; Ward, R.; Mehl, M.; Farrell, C.; Lacroix, J.; Creery, D.; Kesselman, M.; Stanimirovic, D.; Hutchison, J. S.; Group, f. t. C. C. C. T. B. Severe traumatic brain injury in children elevates glial fibrillary acidic protein in cerebrospinal fluid and serum. *Pediatr. Crit. Care Med.* **2011**, *12* (3), 319−324.

(5) Zoltewicz, J. S.; Scharf, D.; Yang, B.; Chawla, A.; Newsom, K. J.; Fang, L. Characterization of antibodies that detect human GFAP after traumatic brain injury. *Biomarker Insights* **2012**, *7*, 71−79.

(6) Unden, J.; Romner, B. Can low serum levels of S100B predict normal CT findings after minor head injury in adults?: an evidence-based review and meta-analysis. *J. Head Trauma Rehabil.* **2010**, *25* (4), 228−240.

(7) North, S. H.; Shriver-Lake, L. C.; Taitt, C. R.; Ligler, F. S. Rapid analytical methods for on-site triage for traumatic brain injury. *Annu. Rev. Anal. Chem.* **2012**, *5* (1), 35−56.

(8) Mondello, S.; Muller, U.; Jeromin, A.; Streeter, J.; Hayes, R. L.; Wang, K. K. W. Blood-based diagnostics of traumatic brain injuries. *Expert Rev. Mol. Diagn.* **2010**, *11* (1), 65−78.

(9) Aoki, Y.; Inokuchi, R.; Gunshin, M.; Yahagi, N.; Suwa, H. Diffusion tensor imaging studies of mild traumatic brain injury: a meta-analysis. *J. Neurol. Neurosurg. Psychiatry* **2012**, *83*, 870−876.

(10) Siman, R.; Toraskar, N.; Dang, A.; McNeil, E.; McGarvey, M.; Plaum, J.; Maloney, E.; Grady, M. S. A panel of neuron-enriched proteins as markers for traumatic brain injury in humans. *J. Neurotrauma* **2009**, *26* (11), 1867−1877.

(11) Anderson, K. J.; Scheff, S. W.; Miller, K. M.; Roberts, K. N.; Gilmer, L. K.; Yang, C.; Shaw, G. The phosphorylated axonal form of the neurofilament subunit NF-H (pNF-H) as a blood biomarker of traumatic brain injury. *J. Neurotrauma* **2008**, *25* (9), 1079−1085.

(12) Papa, L.; Akinyi, L.; Liu, M. C.; Pineda, J. A.; Tepas, J. J. I.; Oli, M. W.; Zheng, W.; Robinson, G.; Robicsek, S. A.; Gabrielli, A.; Heaton, S. C.; Hannay, H. J.; Demery, J. A.; Brophy, G. M.; Layon, J.; Robertson, C. S.; Hayes, R. L.; Wang, K. K. W. Ubiquitin C-terminal hydrolase is a novel biomarker in humans for severe traumatic brain injury. *Crit. Care Med.* **2010**, *38* (1), 138−144.

(13) Honda, M.; Tsuruta, R.; Kaneko, T.; Kasaoka, S.; Yagi, T.; Todani, M.; Fujita, M.; Izumi, T.; Maekawa, T. Serum glial fibrillary acidic protein is a highly specific biomarker for traumatic brain injury in humans compared with S-100B and neuron-specific enolase. *J. Trauma Acute Care Surg.* **2010**, *69* (1), 104−109.

(14) Kochanek, P. M.; Berger, R. P.; Bayr, H.; Wagner, A. K.; Jenkins, L. W.; Clark, R. S. Biomarkers of primary and evolving damage in traumatic and ischemic brain injury: diagnosis, prognosis, probing mechanisms, and therapeutic decision making. *Curr. Opin. Crit. Care* **2008**, *14* (2), 135−141.

(15) Ennen, C. S.; Huisman, T. A. G. M.; Savage, W. J.; Northington, F. J.; Jennings, J. M.; Everett, A. D.; Graham, E. M. Glial fibrillary acidic protein as a biomarker for neonatal hypoxic-ischemic encephalopathy treated with whole-body cooling. *Am. J. Obstet. Gynecol.* **2011**, *205*, 251.e1−7.

(16) Venkatasubbarao, S.; Dixon, C. E.; Chipman, R.; Scherer, A.; Beshay, M.; Kempen, L. U.; Chandra Sekhar, J. G.; Yan, H.; Puccio, A.; Okonkwo, D.; McClain, S.; Gilbert, N.; Vyawahare, S. Field-based multiplex and quantitative assay platforms for diagnostics. *Proc. SPIE* **2011**, 80290P.

(17) Pelinka, L. E.; Kroepfl, A.; Schmidhammer, R.; Krenn, M.; Buchinger, W.; Redl, H.; Raabe, A. Glial fibrillary acidic protein in serum after traumatic brain injury and multiple trauma. *Journal Trauma Acute Care Surg.* **2004**, *57* (5), 1006−1012.

(18) Vos, P. E.; Jacobs, B.; Andriessen, T. M. J. C.; Lamers, K. J. B.; Borm, G. F.; Beems, T.; Edwards, M.; Rosmalen, C. F.; Vissers, J. L. M. GFAP and S100B are biomarkers of traumatic brain injury. *Neurology* **2010**, *75* (20), 1786−1793.

(19) Lumpkins, K. M.; Bochicchio, G. V.; Keledjian, K.; Simard, J. M.; McCunn, M.; Scalea, T. Glial fibrillary acidic protein is highly correlated with brain injury. *J. Trauma Acute Care Surg.* **2008**, *65* (4), 778−784.
(20) Herrmann, M.; Vos, P.; Wunderlich, M. T.; de Bruijn, C. H. M. M.; Lamers, K. J. B. Release of glial tissue-specific proteins after acute stroke. *Stroke* **2000**, *31* (11), 2670−2677.
(21) Niu, L. M.; Lian, K. Q.; Shi, H. M.; Wu, Y. B.; Kang, W. J.; Bi, S. Y. Characterization of an ultrasensitive biosensor based on a nano-Au/DNA/nano-Au/poly(SFR) composite and its application in the simultaneous determination of dopamine, uric acid, guanine, and adenine. *Sens. Actuators, B* **2013**, *178*, 10−18.
(22) Fan, L.; Zhao, G.; Shi, H.; Liu, M.; Li, Z. A highly selective electrochemical impedance spectroscopy-based aptasensor for sensitive detection of acetamiprid. *Biosens. Bioelectron.* **2013**, *43*, 12−18.
(23) Pui, T. S.; Kongsuphol, P.; Arya, S. K.; Bansal, T. Detection of tumor necrosis factor (TNF-α) in cell culture medium with label free electrochemical impedance spectroscopy. *Sens. Actuators, B* **2013**, *181*, 494−500.
(24) Solanki, P. R.; Arya, S. K.; Singh, S. P.; Pandey, M. K.; Malhotra, B. D. Application of electrochemically prepared poly-*N*-methylpyrrole-*p*-toluene sulphonate films to cholesterol biosensor. *Sens. Actuators, B* **2007**, *123* (2), 829−839.
(25) Arya, S. K.; Saha, S.; Ramirez-Vick, J. E.; Gupta, V.; Bhansali, S.; Singh, S. P. Recent advances in ZnO nanostructures and thin films for biosensor applications: review. *Anal. Chim. Acta* **2012**, *737*, 1−21.
(26) Singh, A.; Arya, S. K.; Glass, N.; Hanifi-Moghaddam, P.; Naidoo, R.; Szymanski, C. M.; Tanha, J.; Evoy, S. Bacteriophage tailspike proteins as molecular probes for sensitive and selective bacterial detection. *Biosens. Bioelectron.* **2010**, *26* (1), 131−138.
(27) Mendes, R. K.; Carvalhal, R. F.; Kubota, L. T. Effects of different self-assembled monolayers on enzyme immobilization procedures in peroxidase-based biosensor development. *J. Electroanal. Chem.* **2008**, *612* (2), 164−172.
(28) Arya, S. K.; Wang, K. Y.; Wong, C. C.; Rahman, A. R. A. Anti-EpCAM modified LC-SPDP monolayer on gold microelectrode based electrochemical biosensor for MCF-7 cells detection. *Biosens. Bioelectron.* **2013**, *41*, 446−451.
(29) Arya, S. K.; Solanki, P. R.; Datta, M.; Malhotra, B. D. Recent advances in self-assembled monolayers based biomolecular electronic devices. *Biosens. Bioelectron.* **2009**, *24* (9), 2810−2817.
(30) Arya, S. K.; Prusty, A. K.; Singh, S. P.; Solanki, P. R.; Pandey, M. K.; Datta, M.; Malhotra, B. D. Cholesterol biosensor based on *N*-(2-aminoethyl)-3-aminopropyl-trimethoxysilane self-assembled monolayer. *Anal. Biochem.* **2007**, *363* (2), 210−218.
(31) Pandey, C. M.; Singh, R.; Sumana, G.; Pandey, M. K.; Malhotra, B. D. Electrochemical genosensor based on modified octadecanethiol self-assembled monolayer for *Escherichia coli* detection. *Sens. Actuators, B* **2011**, *151* (2), 333−340.
(32) Vasudev, A.; Kaushik, A.; Bhansali, S. Electrochemical immunosensor for label free epidermal growth factor receptor (EGFR) detection. *Biosens. Bioelectron.* **2013**, *39* (1), 300−305.
(33) Park, M.-K.; Park, J. W.; Oh, J.-H. Optimization and application of a dithiobis-succinimidyl propionate-modified immunosensor platform to detect *Listeria monocytogenes* in chicken skin. *Sens. Actuators, B* **2012**, *171*−*172*, 323−331.
(34) Arya, S. K.; Lee, K. C.; Dah'alan, D. u. B.; Daniel; Rahman, A. R. A. Breast tumor cell detection at single cell resolution using an electrochemical impedance technique. *Lab Chip* **2012**, *12* (13), 2362−2368.
(35) Bai, H.-Y.; Campo, F. J. D.; Tsai, Y.-C. Sensitive electrochemical thrombin aptasensor based on gold disk microelectrodearrays. *Biosens. Bioelectron.* **2013**, *42*, 17−22.
(36) Arya, S. K.; Chornokur, G.; Venugopal, M.; Bhansali, S. Dithiobis(succinimidyl propionate) modified gold microarray electrode based electrochemical immunosensor for ultrasensitive detection of cortisol. *Biosens. Bioelectron.* **2010**, *25* (10), 2296−2301.
(37) Szymańska, I.; Radecka, H.; Radecki, J.; Kaliszan, R. Electrochemical impedance spectroscopy for study of amyloid β-peptide interactions with (−) nicotine ditartrate and (−) cotinine. *Biosens. Bioelectron.* **2007**, *22* (9−10), 1955−1960.

dx.doi.org/10.1021/la401109r | *Langmuir* XXXX, XXX, XXX−XXX